Virologica Sinica xxx (xxxx) xxx

Contents lists available at ScienceDirect

Virologica Sinica

journal homepage: www.keaipublishing.com/en/journals/virologica-sinica
www.virosin.org

Research Article

Establishment and application of a surrogate model for human Ebola virus disease in BSL-2 laboratory

Wanying Yang [a,b,1], Wujian Li [b,c,1], Wujie Zhou [b,1], Shen Wang [b], Weiqi Wang [b,c], Zhenshan Wang [b,d], Na Feng [b], Tiecheng Wang [b], Ying Xie [a,*], Yongkun Zhao [b,*], Feihu Yan [b,*], Xianzhu Xia [b]

[a] Hebei Key Lab of Laboratory Animal Science, Department of Laboratory Animal Science, Hebei Medical University, Shijiazhuang, 050017, China
[b] Key Laboratory of Jilin Province for Zoonosis Prevention and Control, Changchun Veterinary Research Institute, Chinese Academy of Agricultural Sciences, Changchun, 130122, China
[c] College of Veterinary Medicine, Jilin University, Changchun, 130062, China
[d] College of Veterinary Medicine, Jilin Agricultural University, Changchun, 130118, China

ARTICLE INFO

Keywords:
Ebola virus (EBOV)
Recombinant vesicular stomatitis virus
Pathogenicity
Syrian hamster
Surrogate models
Vaccine evaluation and drug screening

ABSTRACT

The Ebola virus (EBOV) is a member of the *Orthoebolavirus* genus, *Filoviridae* family, which causes severe hemorrhagic diseases in humans and non-human primates (NHPs), with a case fatality rate of up to 90%. The development of countermeasures against EBOV has been hindered by the lack of ideal animal models, as EBOV requires handling in biosafety level (BSL)-4 facilities. Therefore, accessible and convenient animal models are urgently needed to promote prophylactic and therapeutic approaches against EBOV. In this study, a recombinant vesicular stomatitis virus expressing Ebola virus glycoprotein (VSV-EBOV/GP) was constructed and applied as a surrogate virus, establishing a lethal infection in hamsters. Following infection with VSV-EBOV/GP, 3-week-old female Syrian hamsters exhibited disease signs such as weight loss, multi-organ failure, severe uveitis, high viral loads, and developed severe systemic diseases similar to those observed in human EBOV patients. All animals succumbed at 2–3 days post-infection (dpi). Histopathological changes indicated that VSV-EBOV/GP targeted liver cells, suggesting that the tissue tropism of VSV-EBOV/GP was comparable to wild-type EBOV (WT EBOV). Notably, the pathogenicity of the VSV-EBOV/GP was found to be species-specific, age-related, gender-associated, and challenge route-dependent. Subsequently, equine anti-EBOV immunoglobulins and a subunit vaccine were validated using this model. Overall, this surrogate model represents a safe, effective, and economical tool for rapid preclinical evaluation of medical countermeasures against EBOV under BSL-2 conditions, which would accelerate technological advances and breakthroughs in confronting Ebola virus disease.

1. Introduction

Ebola virus (EBOV), a member of *Orthoebolavirus* genus, *Filoviridae* family, causes severe hemorrhagic fever in human and non-human primates (NHPs). Among the six species in *Orthoebolavirus* genus, Ebola virus is the most lethal pathogen, resulting in the largest outbreak. It caused 28,646 cases and 11,323 deaths in multiple countries between 2013 and 2016 since the discovery of EBOV in 1976 (Coltart et al., 2017). EBOV is transmitted from wild animals to people and spreads through contact with infected blood, tissues, organs, other bodily fluids, and contaminated items (Jacob et al., 2020). After an incubation period ranging from 2 to 21 days, the disease symptoms begin suddenly, including fever, headache, and sore throat. This is followed by rash, vomiting, diarrhea, and in severe cases, multi-organ failure, hemorrhage, and death (Baseler et al., 2017; Jacob et al., 2020; Leligdowicz et al., 2016). Ebola viruses are non-segmented single-stranded negative-sense RNA viruses with a genome size of 18.9 kb. They have eight sub genomic mRNAs encoding seven structural proteins (Feldmann et al., 2020). Among these proteins, the membrane-associated protein (glycoprotein, GP) is responsible for viral attachment to target cells, viral entry into cells, membrane fusion, and eliciting a protective antibody response. Thus, it is the primary target for studying the pathogenesis of EBOV and

* Corresponding authors.
E-mail addresses: xieying@hebmu.edu.cn (Y. Xie), zhaoyongkun1976@126.com (Y. Zhao), yanfh1990@163.com (F. Yan).
[1] Wanying Yang, Wujian Li, and Wujie Zhou contributed equally to this work.

https://doi.org/10.1016/j.virs.2024.03.010
Received 17 November 2023; Accepted 22 March 2024

developing preventative vaccines and therapeutic antibodies against EBOV (Martin et al., 2016, 2017).

Animal models that accurately mimic Ebola virus disease (EVD) in humans are urgently needed to fully uncover the pathogenesis and transmission mechanism and to be better prepared for potential outbreaks of EBOV. Several infection models of EVD have been established, including mice, guinea pigs, ferrets, Syrian hamsters, and NHPs (Bente et al., 2009; Bradfute et al., 2012; Bray et al., 1999; Connolly et al., 1999; Geisbert et al., 2002; Kozak et al., 2016; Wahl-Jensen et al., 2012; Yan et al., 2019). The NHP model is the gold standard of EVD as it closely mimics human infection (Nakayama and Saijo, 2013). However, ethical issues, costs, experimental facilities, and the availability of reagents limit the application of NHPs. Mice, hamsters, and guinea pigs were resistant to wild-type EBOV (WT EBOV) infection; therefore, virus adaption should be conducted to accomplish effective infection, which is time-consuming and introduces additional mutants (Bray et al., 1999; Connolly et al., 1999; Ebihara et al., 2013). In contrast, ferrets, an alternative small animal model for NHPs, are naturally susceptible to WT EBOV (Cross et al., 2016). Immunocompromised mice (IFN-α/β receptor-knockout (*IFNAR*$^{-/-}$) and transcription factor STAT1-knockout (*STAT1*$^{-/-}$) mice) are also used as surrogate models since they are highly susceptible to WT EBOV(Bray, 2001). However, these naturally susceptible models should be conducted in BSL-4, which limits the preclinical screening of anti-EBOV drugs. In comparison, surrogate models enable the simulation of EVD symptoms and the screening of medical countermeasures under BSL-2, which is more feasible and economical.

In this study, a recombinant vesicular stomatitis virus bearing the glycoprotein of EBOV was rescued, termed VSV-EBOV/GP, which serves as a surrogate virus for EBOV infection in hamsters. VSV-EBOV/GP infection results in fatal infection in age, gender, and challenge route-dependent manners, and exhibits several critical aspects of human in hamsters. Additionally, the efficacy of equine anti-EBOV immunoglobulins and a subunit vaccine have been evaluated in this model. Overall, this study provides a valuable tool for screening vaccines and antibodies under BSL-2 conditions.

2. Materials and methods

2.1. Cells, viruses, and antibodies

Vero E6 cells (ATCC® CRL-1587™) were stored at the Changchun Veterinary Institute and cultured in Dulbecco's Modified Eagle's Medium (DMEM, Gibco, Grand Island, NY, USA) containing 10% fetal bovine serum (FBS, Gibco, Thermo Fisher Scientific, MA, USA), and 1% Penstrep in a 37 °C, 5% CO_2 incubator for the duration of culture. Recombinant vesicular stomatitis viruses were generated by replacing the VSV glycoprotein with full-length GPs from Ebola virus (Genbank NO. AF086833.2), Sudan virus (Genbank NO. NC_006432.1) and Lassa virus (Genbank NO. HQ688672.1), termed as VSV-EBOV/GP, VSV-SUDV/GP and VSV-LASV/GP, and were passaged in Vero E6 cells and stored at −80 °C. Wild-type VSV (WT VSV) (Genbank NO. OR712768.1), murine anti-EBOV antibody, equine anti-EBOV immunoglobulins and a subunit vaccine (EBOV GP Δmuc) (truncated forms of EBOV GP) (amino acids 1 to 311 linked through an aspartic acid to residues 464 to 637) were stored at the Changchun Veterinary Institute. Subunit vaccines are designed and expressed as previously described (Keck et al., 2016).

2.2. Construction and rescue of VSV-EBOV/GP

The VSV full-length plasmid, named p3.1-VSV-eGFP, was constructed in the pcDNA3.1 vector as described previously (Wang et al., 2022). A recombinant full-length plasmid (named p3.1-VSVΔG-EBOV GP) was generated by replacing the VSV glycoprotein with full-length GPs from Ebola virus (AF086833.2) and inserting an enhanced green fluorescence (eGFP) reporter gene between the N and P genes. The generation of pcDNA3.1-VSV-N, pcDNA3.1-VSV-P, pcDNA3.1-VSV-L, and pcDNA3.1-VSV-G plasmids were performed as previously described and stored at −80 °C (Wang et al., 2022). The p3.1-VSVΔG-EBOV GP and four adjuvant plasmids were co-transfected into BSR/T7 cells. The procedure was carried out in accordance with the calcium phosphate transfection kit instructions (Invitrogen, Waltham, MA, USA). Recombinant virus rescue was determined by cytopathological effects and expression of eGFP reporter genes. Recombinant viruses were passaged on Vero E6 cells (Fig. 1A).

2.3. In vitro growth kinetic of viruses

Vero E6 cells were cultured overnight in 24-well plates and infected with WT VSV, VSV-EBOV/GP, VSV-SUDV/GP, and VSV-LASV/GP, respectively, at an MOI of 0.1. The cell culture supernatants were harvested at 12, 24, 48, 60, 72, 84, and 96 hpi (hours post-infection), respectively, and then the viral titers were calculated using the Reed-Muench method. Finally, growth curves were outlined based on the viral titers of the viruses at different times (Fig. 1B).

2.4. Virus inoculation of animals

Syrian hamsters, BALB/c mice, and Sprague-Dawley (SD) rats were purchased from Beijing Vital River Laboratory Animal Technology Company Limited (Peking, CN). Hartley guinea pigs were purchased from Beijing Keyu Animal Breeding Center (Peking, CN). All animals were housed in a special pathogen-free facility with a 12:12-h light-dark cycle, on sterile chow and sterilized water.

In common rodent infection experiment, four groups (n = 5 per group) of 3-week-old female SD rats, BALB/c mice, guinea pigs, or Syrian hamsters were intraperitoneally inoculated with 10^7 tissue culture infective dose ($TCID_{50}$) of VSV-EBOV/GP, while animals in control groups were intraperitoneally injected with the same volume of PBS. Further, twenty 3-week-old female Syrian hamsters were randomly divided into four groups and inoculated intraperitoneally with 10^7 $TCID_{50}$ of WT-VSV, VSV-EBOV/GP, VSV-SUDV/GP, and VSV-LASV/GP, respectively.

In the assessment of the effect of gender on the lethality of VSV-EBOV/GP infection in Syrian hamsters, groups of 3-week-old female and male Syrian hamsters (n = 10 per group) inoculated intraperitoneally with 10^7 $TCID_{50}$ of VSV-EBOV/GP. After 36 h infection, blood samples were collected through the orbital venous plexus and analyzed with complete blood count and blood chemistry. In order to assess systemic viral spread to different organs, heart, liver, spleen, lung, kidney, stomach, intestine, and brain were collected, and analyzed pathologies and viral distributions.

In the evaluation of the effect of age on the lethality of VSV-EBOV/GP infection in Syrian hamsters, 3-week-old, 3-month-old, and 1-year-old female and male Syrian hamsters (n = 8 per group) were inoculated intraperitoneally with 10^7 $TCID_{50}$ of VSV-EBOV/GP, while animals in control groups were intraperitoneally injected with the same volume of PBS. After 36 h infection, three animals in each group were sacrificed, liver and spleen were collected and used to determine viral loads.

In the appraisal of the impact of challenge route on the lethality of VSV-EBOV/GP infection in Syrian hamsters, four groups of 3-week-old female Syrian hamsters (n = 8 per group) infected with 10^7 $TCID_{50}$ of VSV-EBOV/GP via intraperitoneal (i.p.), subcutaneous (s.c.), intramuscular (i.m.), or intranasal (i.n.) route. After 36 h infection, blood samples were collected through the orbital venous plexus and analyzed with complete blood count and blood chemistry. Meanwhile, internal organs were harvested and assessed for viral titers and pathologies, including the liver, lung, spleen, and kidney.

All animals were monitored daily for signs of disease, including changes in weight, physical activity, and food and water intake.

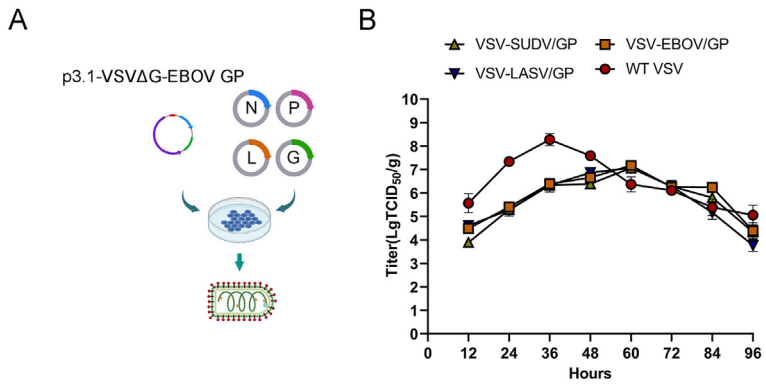

Fig. 1. A Scheme diagram of the generation of recombinant vesicular stomatitis virus VSV-EBOV/GP. The recombinant full-length plasmid (p3.1-VSVΔG-EBOV GP) and four helper plasmids (pcDNA3.1-VSV-N, pcDNA3.1-VSV-P, pcDNA3.1-VSV-L, and pcDNA3.1-VSV-G) were co-transfected into BSR/T7 cells and obtained a recombinant virus bearing the glycoprotein of EBOV. **B** One-step growth curves of WT VSV, VSV-EBOV/GP, VSV-SUDV/GP, and VSV-LASV/GP. WT VSV, VSV-EBOV/GP, VSV-SUDV/GP, and VSV-LASV/GP were inoculated into Vero E6 cells at an MOI of 0.1. Viruses were collected at 12 h intervals to measure titers.

2.5. Quantification of viral loads by $TCID_{50}$

Vero E6 cells were plated in 100 μL of complete DMEM media in a 96-well plate to target confluency of 70%–90% at 24 h after plating. Organs were homogenized and cleared of cellular debris by centrifugation. The supernatant was serially diluted at a tenfold ratio, and 100 μL was added to 96-well cell culture plates. The plates were incubated at 37 °C for 1 h and then washed thrice with sterile PBS. 100 μL of incomplete medium containing 2% FBS and 1% penicillin-streptomycin was added to each well of 96-well plate. The median $TCID_{50}$ was calculated by observing the number of wells with cytopathic effect (CPE) based on the Reed and Muench method after incubating for 72 h (Manangeeswaran et al., 2016).

2.6. Hematological tests

Blood samples were collected through the orbital venous plexus into anticoagulant tubes containing EDTAK2 and heparin to determine Syrian hamsters' complete blood count and blood biochemical parameters. A complete blood count was carried out under the automatic blood analyzer (BC-5000vet, Mindray, CN), and the operation procedures were carried out according to the instrument's operation instructions.

2.7. Histopathology and immunohistochemistry

Syrian hamsters were euthanized at the appointed time. Heart, liver, spleen, lung, kidney, stomach, intestine, and brain were collected. Tissue samples were fixed in 10% neutral buffered formalin. Samples were cut, paraffin-embedded, sectioned with a 5 μm slicer, placed on slides, and stained with hematoxylin and eosin (H&E) for histopathological examination. For immunohistochemistry (IHC), quenching of paraffin-embedded tissues was performed with 3% hydrogen peroxide in methanol for 10 min, and specific anti-EBOV GP immunoreactivity was detected using murine anti-EBOV antibody as the primary antibody. After incubation with primary antibody, sections were washed with PBS 3 times and species-matched secondary antibodies were applied for 2 h at 4 °C. The brown color represents the immunoreactivity of the tissue sections. The histopathology and immunohistochemistry assays were performed as previously described (Cooper et al., 2018). Pathological scores by the International Norms for the Terminology of Pathological Changes and Diagnostic Criteria in Rats and Mice (INHAND). Histochemical score IRS=SI (strength of positivity) × PP (percentage of positive cells). SI is classified into three levels, with no positive coloring in level 0, weakly positive yellowish in level 1, moderately positive brownish yellow in level 2, and strongly positive brownish brown in level 3; PP is classified into four levels, with 0–5% in level 0, 6%–25% in level 1, 26%–50% in level 2, 51%–75% in level 3, and >75% in level 4 (Xie et al., 2014). Percentage of positive cells = number of positive cells/total number of cells (Benonisson et al., 2019).

2.8. Virus neutralization assays

EBOV-specific virus neutralization antibody (VNA) titers were analyzed in serum samples collected from immunized hamsters using a neutralization assay. Briefly, serum samples were complement-inactivated at 56 °C for 30 min and serially diluted two-fold (Syrian hamster sera, from 1:8) in cell culture medium, 100 μL of diluted serum samples were added to a 96-well plate, and 100 $TCID_{50}$ VSV-EBOV/GP was added to each well and incubated at 37 °C for 1 h and then added 1×10^4 Vero E6 cells into each well. Virus-only control wells and uninfected-cell control wells were also included in the plate. CPE was detected under a microscope after the cells were cultured at 37 °C in 5% CO_2 for 48–72 h. The neutralizing antibody titers were defined as the inverse of the highest dilution, which could completely inhibit the production of the CPE compared with viral controls.

2.9. Evaluation of equine anti-EBOV immunoglobulins and EBOV GP Δmuc in Syrian hamster model

Thirty-three female 3-week-old Syrian hamsters were randomized into three groups. Each hamster was intraperitoneally given 5 mg of equine anti-EBOV immunoglobulins. In the prevention group, Syrian hamsters were first intraperitoneally given 5 mg purified equine anti-EBOV immunoglobulins and challenged by i.p. administration of 10^7 $TCID_{50}$ VSV-EBOV/GP in 1 mL DMEM after 24 h. In the treatment group, Syrian hamsters were first challenged with 10^7 $TCID_{50}$ VSV-EBOV/GP in 1 mL DMEM and given 5 mg anti-EBOV equine immunoglobulins via the i.p. route injection 24 h post-infection. The treatment was carried out for the control group with an equal volume of PBS.

Twenty-two female 3-week-old Syrian hamsters were randomized into two groups. Each hamster was immunized intraperitoneally with 5 mg EBOV GP Δmuc in 50 μL PBS mixed with equal volume Freund's complete adjuvant (Thermo Fisher Scientific, USA). Hamsters in the control group were given an equivalent volume of PBS. All groups received a second and third identical vaccination one week and three weeks after the primary immunization. Blood samples were collected through the orbital venous plexus at different time points post-immunization, and serum was separated and stored at −80 °C for antibody titration.

At 3 dpi and 5 dpi, three hamsters in each group were sacrificed. Liver tissue from euthanized animals was harvested to test the viral loads,

histopathology, and immunohistochemistry tests. All animals were monitored for clinical signs of disease, percent of survival, and weight change.

2.10. Statistical analysis

GraphPad Prism v9.0 (GraphPad Software Inc. San Diego, CA, USA) was used to analyze the data, which were expressed as mean standard error of mean (SEM). To assess changes in complete blood count and liver parameters, we performed a one-way repeated measures analysis of variance (ANOVA) followed by a paired *t*-test comparing mean blood counts and liver parameters. $p < 0.05$ was considered a statistically significant difference. *, $P < 0.05$; **, $P < 0.01$; ***, $P < 0.001$; ****, $P < 0.0001$.

3. Results

3.1. Syrian hamsters were uniformly lethal to the VSV-EBOV/GP infection

To explore the lethality of VSV-EBOV/GP to different rodents, five SD rats, Hartley guinea pigs, BALB/c mice or Syrian hamsters in each group were inoculated with 10^7 $TCID_{50}$ of VSV-EBOV/GP via the i.p. route. Post-inoculation, animals in each group were monitored daily for clinical signs of EVD. At the end-point of the experiment, SD rats, Hartley Guinea Pigs, and BALB/c mice survived and exhibited significant weight loss of 5%–15% at 1–2 dpi, and the overall body weight gain were lower than control groups (Fig. 2A–**2C**). However, infected Syrian hamsters showed a significant weight loss of 15% and succumbed to the disease at 2–3 dpi whereas Syrian hamsters in control group survived, and were euthanized as planned at the scheduled end of project at 10 dpi (Fig. 2D). To exclude the potential pathogenicity of VSV backbone, four groups of Syrian hamsters were further inoculated with WT-VSV, VSV-SUDV/GP, VSV-LASV/GP, and VSV-EBOV/GP via i.p. route, respectively. All animals in VSV-EBOV/GP-infected group, not those in VSV-SUDV/GP or VSV-LASV/GP-infected group, succumbed to the disease at 3 dpi. Only one Syrian hamster survived for the WT VSV infection group (Fig. 2E). These results suggest that WT VSV is lethal to Syrian hamsters, but the pathogenicity of recombinant virus based on VSV virus vector depends on exogenous glycoproteins carried, VSV-EBOV/GP could be further investigated as a lethal surrogate virus model for EBOV in Syrian hamsters.

3.2. Characterization of the 3-week-old Syrian hamsters infected with VSV-EBOV/GP

To reveal the gender-associated pathogenicity of the VSV-EBOV/GP, groups of five female and male Syrian hamsters were inoculated via the i.p. route with VSV-EBOV/GP at a dose of 10^7 $TCID_{50}$ (Fig. 3A). All female Syrian hamsters showed decreased rectal temperature and 10%–18% weight loss and died at 2–3 dpi, while only three of five male Syrian hamsters lost 15% weight and succumbed to the disease at 1.5–3.5 dpi. At the project's end at 10 dpi, two male Syrian hamsters survived and gained 20% more weight than pre-infection (Fig. 3B).

Further, for hematological analysis, blood samples from animals infected with VSV-EBOV/GP were collected one day before and 36 h post-infection. Specifically, increases in concentrations of alkaline phosphatase (ALP) and aminotransferase (ALT) and a decrease in albumin (ALB) were observed, indicating liver damage or other pancreas-related disorders (Fig. 3C). A moderate increase in white blood cell (WBC) count and the percentage of granulocytes (GRAN%), with significant decreases in platelet count (PLT) and a medium decrease in the percentage of lymphocytes (LYM%), was also observed, indicating the severe viral infections and blood clotting disorders (Fig. 3D). Overall, the disease process in hamsters showed many similarities to that observed in NHPs and EVD patients (Jacob et al., 2020; Johnson et al., 2023).

To investigate the replication of VSV-EBOV/GP in Syrian hamsters' multiple organs or tissues such as heart, liver, spleen, lung, kidney, stomach, intestine, and brain were harvested at 36 h post-infection to quantify viral titers by $TCID_{50}$. VSV-EBOV/GP were detected in heart, liver, spleen, lung, kidney, stomach, intestines and brain tissues, with a mean viral load range of $10^{3.8}$ to $10^{8.2}$ $TCID_{50}$ per gram of tissue. The highest viral loads were found in the liver ($10^{8.2}$ $TCID_{50}$/g), and the lowest levels were found in the brain ($10^{3.8}$ $TCID_{50}$/g) (Fig. 3E).

Further, the gross pathology and histological assays were performed to check the pathological changes in the liver, spleen, lung, and kidney at 36 h post-infection. Viral antigens were identified in liver, hepatocyte necrosis, nuclear fragmentation, and marked inflammation were observed. In the spleen, abundant amounts of viral antigen were detected within macrophages, and throughout the white pulp and red pulp areas. Pathological findings showed multiple lymphocytic necrosis with nuclear fragmentation, and neutrophilic infiltrate. Moreover, capillary cells were predominantly present with virus-positive antigens, and the lung was characterized by mild thickening of the diffuse alveolar walls and narrowing or loss of alveolar lumens, accompanied by a large inflammatory cellular infiltrate. A few lesions were observed in the epithelial cells of the renal tubules in the kidney (Fig. 3G and H).

Notably, VSV-EBOV/GP-infected Syrian hamsters developed secretions in their eyes, which impaired their vision and covered the surface of the eyeballs (Fig. 3F). It has been demonstrated that survivors of Ebola disease are at risk for ocular complications, such as uveitis and optic neuropathy, which lead to secondary structural complications, visual impairment, and blindness (Shantha et al., 2017). It is a sign that 3-week-old Syrian hamsters infected with VSV-EBOV/GP have the possibility of playing a role in the study of optic nerve disorders caused by EVD.

In conclusion, 3-week-old Syrian hamsters infected with VSV-EBOV/GP show a rapid onset of symptoms, are predominantly hepatophilic, cause systemic infection, and develop severe systemic diseases similar to those observed in human EBOV patients. More importantly, female Syrian hamsters have more uniform lethality and morbidity than males.

3.3. Age-related lethality in VSV-EBOV/GP infected Syrian hamsters

To further explore the characterization of the lethal model for VSV-EBOV/GP infection in Syrian hamsters, we evaluated the lethality of Syrian hamsters of different genders and ages following infection with VSV-EBOV/GP. It has been shown that 3-week-old female Syrian hamsters had more uniform lethality of VSV-EBOV/GP infection than males, died within 2–3 dpi, and had a significant 10%–18% weight loss. (Fig. 4A). In contrast, there was no mortality after infection with VSV-EBOV/GP on either 3-month-old or 1-year-old hamsters; all the hamsters lost weight (~7% loss of group mean body weight on 3 months hamsters and ~10% on 1-year-old hamsters) but recovered to their original weights by day 3 and 5 post-challenge (Fig. 4B and C). Overall, the liver had a higher viral load than the spleen; Syrian hamsters in the 3-week-old group had the highest viral loads; and the viral load in females were higher than males at 3 dpi. Those in the 3-month-old group had the lowest viral loads and recovered quickly from the infection, as evidenced by the fast rate of body weight gain (Fig. 4D). The above results suggest that 3-week-old female Syrian hamsters are the most uniformly lethal model in VSV-EBOV/GP infection.

3.4. Challenge route-dependent lethality in VSV-EBOV/GP infected Syrian hamsters

To investigate differences in lethality of Syrian hamsters infected via different routes of infection with VSV-EBOV/GP, 3-week-old female hamsters were infected via i.p., s.c., i.m., and i.n. route. The results showed that Syrian hamsters injected intraperitoneally succumbed at 2.5

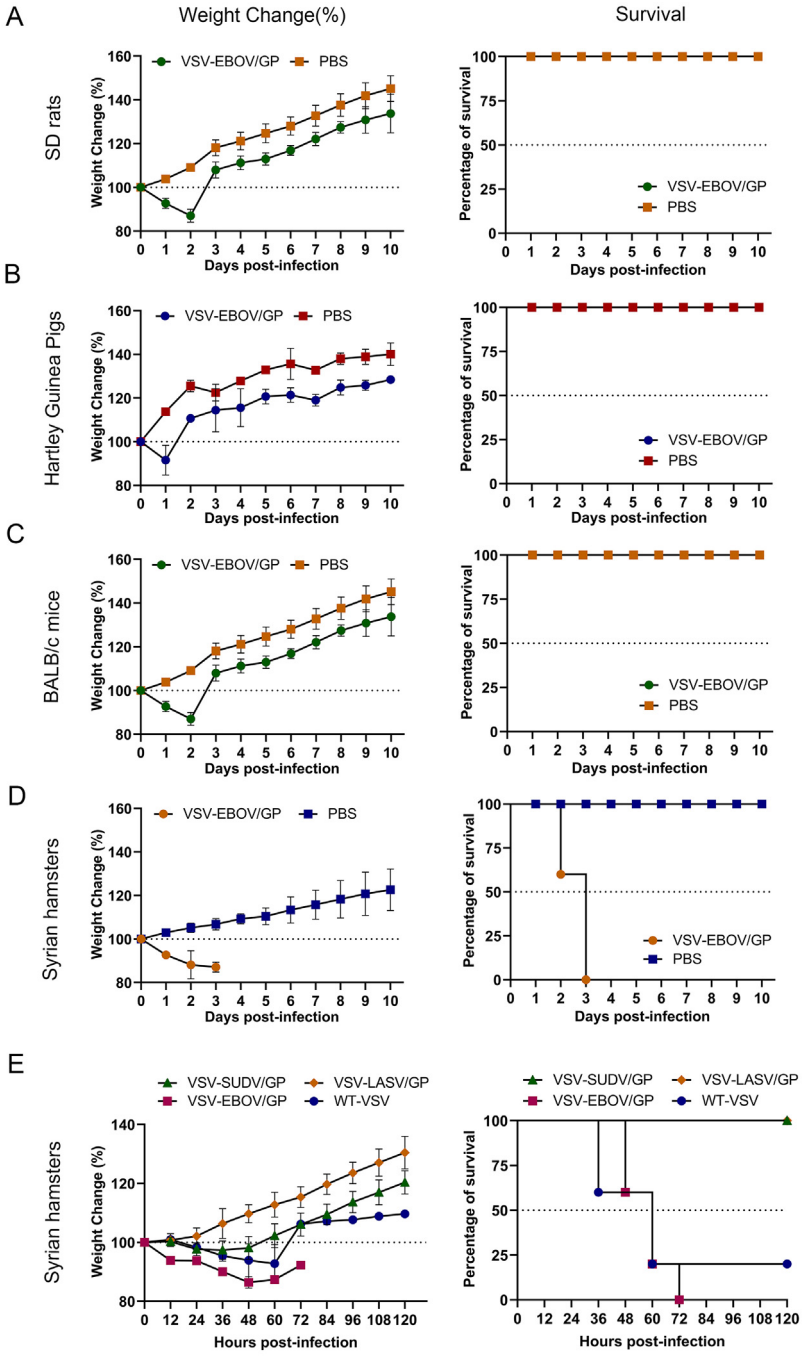

Fig. 2. Weight change and percent of survival in rodents of VSV-EBOV/GP infection. Sprague-Dawley (SD) rats (**A**), Hartley guinea pigs (**B**), BALB/c mice (**C**), Syrian hamsters (**D**) were inoculated with VSV-EBOV/GP (10^7 $TCID_{50}$) via intraperitoneal (i.p.) route. Weight change and percent of survival were monitored. **E** Weight change and percent of survival were monitored in Syrian hamsters inoculated with WT-VSV, VSV-SUDV/GP, VSV-LASV/GP, and VSV-EBOV/GP via i.p. route.

dpi and weight loss of 10%–15%, while those infected subcutaneously, intramuscularly, and intranasally resulted in weight loss followed by gradual recovery (Fig. 5A). Blood biochemical analyses were similar to those observed for human EBOV disease (Nicastri et al., 2019). Specifically, there was an increase in concentrations/activities of ALP, ALT, WBC, and GRAN%, but a decrease in ALB, PLT, and LYM% was observed. The most pronounced changes were observed in the i.p. infection group (Fig. 5B). Additionally, viral loads were determined in the liver, spleen, lung, and kidney tissues of each group of hamsters and were highest in the i.p. infection group. Overall, viral loads in the liver were slightly higher (Fig. 5C). Meanwhile, i.p. infection group had the most severe lesions with massive inflammatory cell infiltration, lymphocytic necrosis, and viral antigens in the liver, spleen, lungs, and kidneys compared to other groups (Fig. 5D and F). Pathological and histochemical scores were also the most severe in the i.p. infection group (Fig. 5E and G). The above results indicate that among various infection routes tried, only the i.p. route resulted in lethal disease in hamsters.

3.5. *Preventive and therapeutic effects of equine anti-EBOV immunoglobulins in lethal Syrian hamster model*

The availability of this lethal model was demonstrated by evaluating the preventive and therapeutic effects of equine anti-EBOV immunoglobulins. The hamsters were injected with 5 mg hyperimmune equine

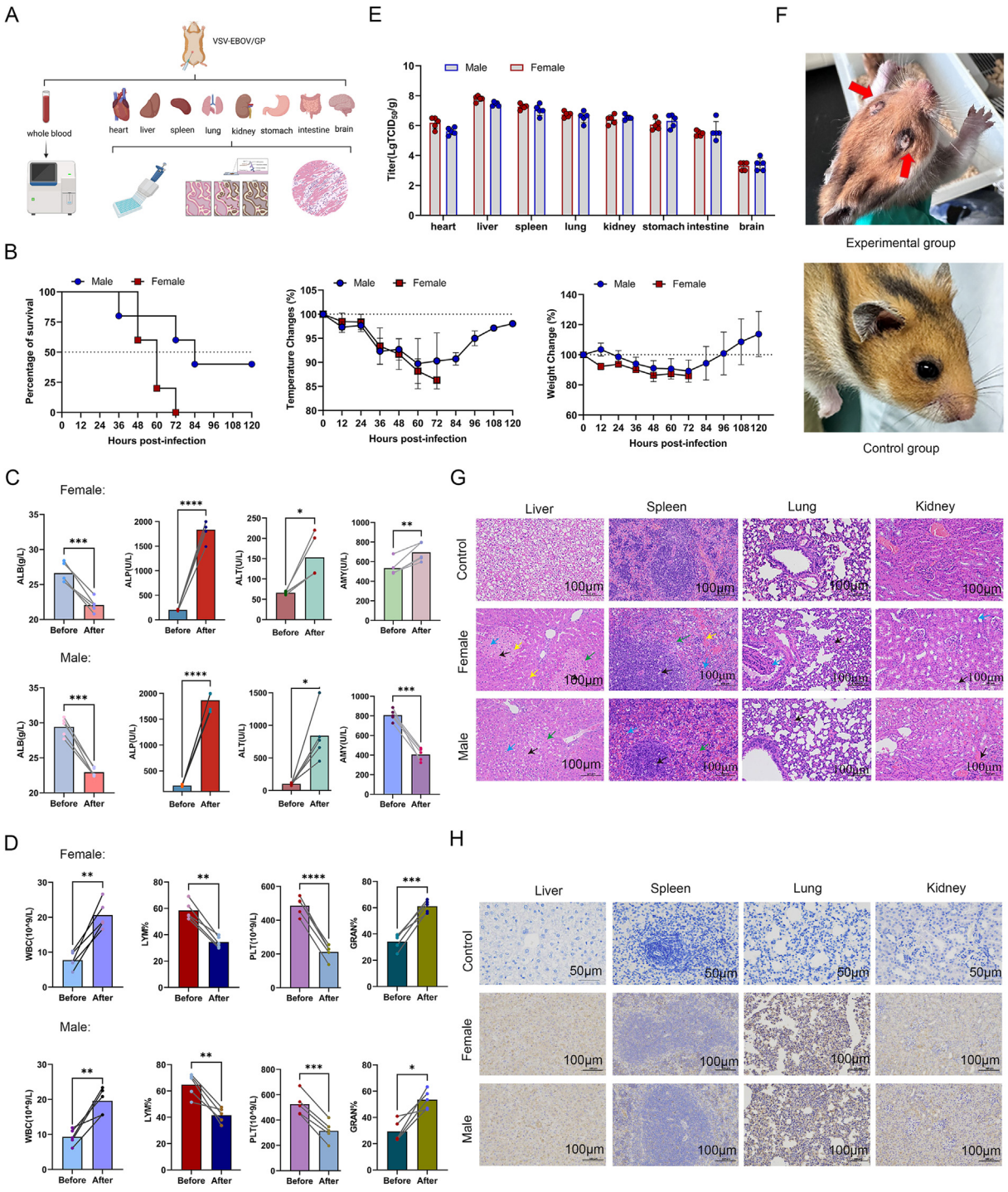

Fig. 3. Characterization of VSV-EBOV/GP infection in 3-week-old Syrian hamsters. **A** Three-week-old Syrian hamsters were intraperitoneally infected with VSV-EBOV/GP (10^7 $TCID_{50}$). **B** Animals were monitored for weight changes, temperature changes, and survival. **C, D** Blood biochemistry and blood cell count were analyzed at 1.5 days post-infection. **E** Viral loads including hearts, livers, spleens, lungs, kidneys, stomachs, intestines, and brains were determined at 1.5 days post-infection. Data presented as mean ± SEM. Statistical analyses were performed using One-way ANOVA. *, $P < 0.05$; **, $P < 0.01$; ***, $P < 0.001$; ****, $P < 0.0001$. **F** Severe uveitis was observed in the eyes of VSV-EBOV/GP infected animals. **G, H** Histopathological and immunohistochemistry assays of the liver, spleen, lung and kidney at 1.5 days post-infection. Scale bar = 100 μm. Hepatic lesions including hepatocellular necrosis, nuclear fragmentation (black arrows), lymphocytic infiltration (blue arrows), granulocytic infiltration (green arrows), and hepatocellular steatosis (yellow arrows) were observed. Splenic lesions including lymphocytic necrosis with nuclear fragmentation (black arrows), cellular necrosis with nuclear fragmentation (blue arrows), neutrophilic infiltrate (green arrows), and bruising (yellow arrows) were observed. Lung tissue showed diffuse mild thickening of the alveolar wall, narrowing or loss of the alveolar lumen with inflammatory cell infiltration (black arrows); bronchial epithelial cells were detached (blue arrows). Kidney lesions were seen as hydropic degeneration of renal tubular epithelial cells (black arrows) and dilatation of renal tubular interstitial vessels seen as stasis (blue arrows).

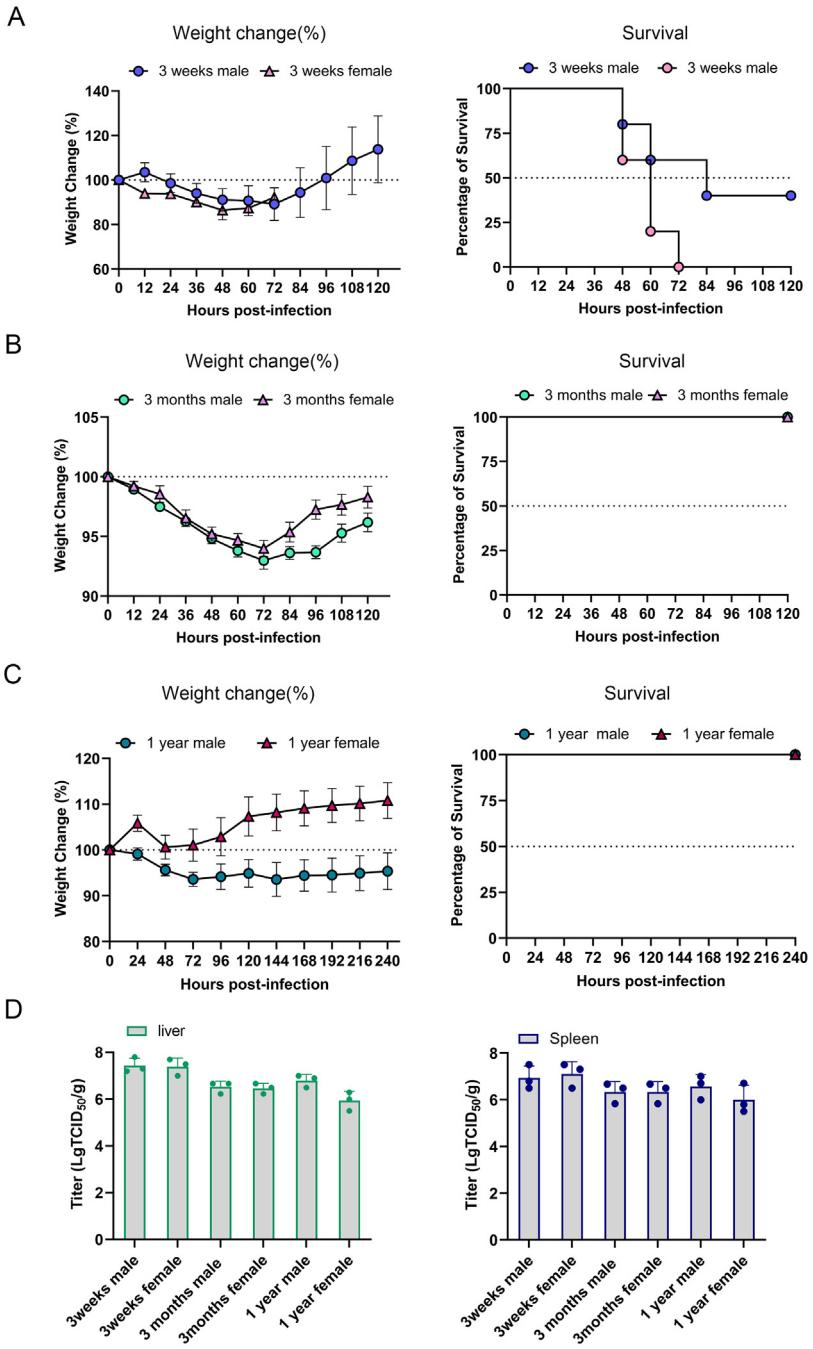

Fig. 4. Comparison of age-related and gender-associated of Syrian hamster infected with VSV-EBOV/GP. 3-week-old (**A**), 3-month-old (**B**) and 1-year-old (**C**) Syrian hamsters were infected with VSV-EBOV/GP (10^7 $TCID_{50}$) via intraperitoneal route. Weight change and percent survival were monitored. Viral loads were evaluated by $TCID_{50}$ in the liver and spleen at 3 days post-infection (**D**).

immunoglobulin via i.p. route one day before or after the VSV-EBOV/GP inoculation. Weight changes and survival were followed for 15 days, and livers were harvested at 3 dpi and 5 dpi for viral loads, histopathology and immunohistochemistry analysis (Fig. 6A). Hamsters treated with PBS succumbed at 2–3 dpi. In contrast, the hamsters in the treatment group lost 15% weight within 3 dpi and gradually regained in following 12 days, while the prevention group consistently gained weight at 20%–60% (Fig. 6B) and progressively reduced viral burden levels in the liver compared to the attack control group (Fig. 6C). For the attack group, liver tissue showed severe liver damage, necrosis, nuclear fragmentation, and lymphocytic infiltration, while the treatment and prevention groups exhibited significantly reduced lesions (Fig. 6E). The treatment and prevention groups also had significantly fewer viral antigens than the attack group (Fig. 6F). The result of the neutralization assay we measured that the equine anti-EBOV immunoglobulins have complete neutralizing activity against VSV-EBOV/GP at a concentration of 0.15 (μg/mL) (Fig. 6D). These results showed that Syrian hamsters can serve as a tool for evaluating equine anti-EBOV immunoglobulins' preventive and therapeutic effectiveness.

3.6. *Preventive effects of EBOV GP Δmuc in lethal Syrian hamster model*

The practicality of this lethal model was proved by evaluating the preventive effects of EBOV GP Δmuc, a subunit candidate vaccine

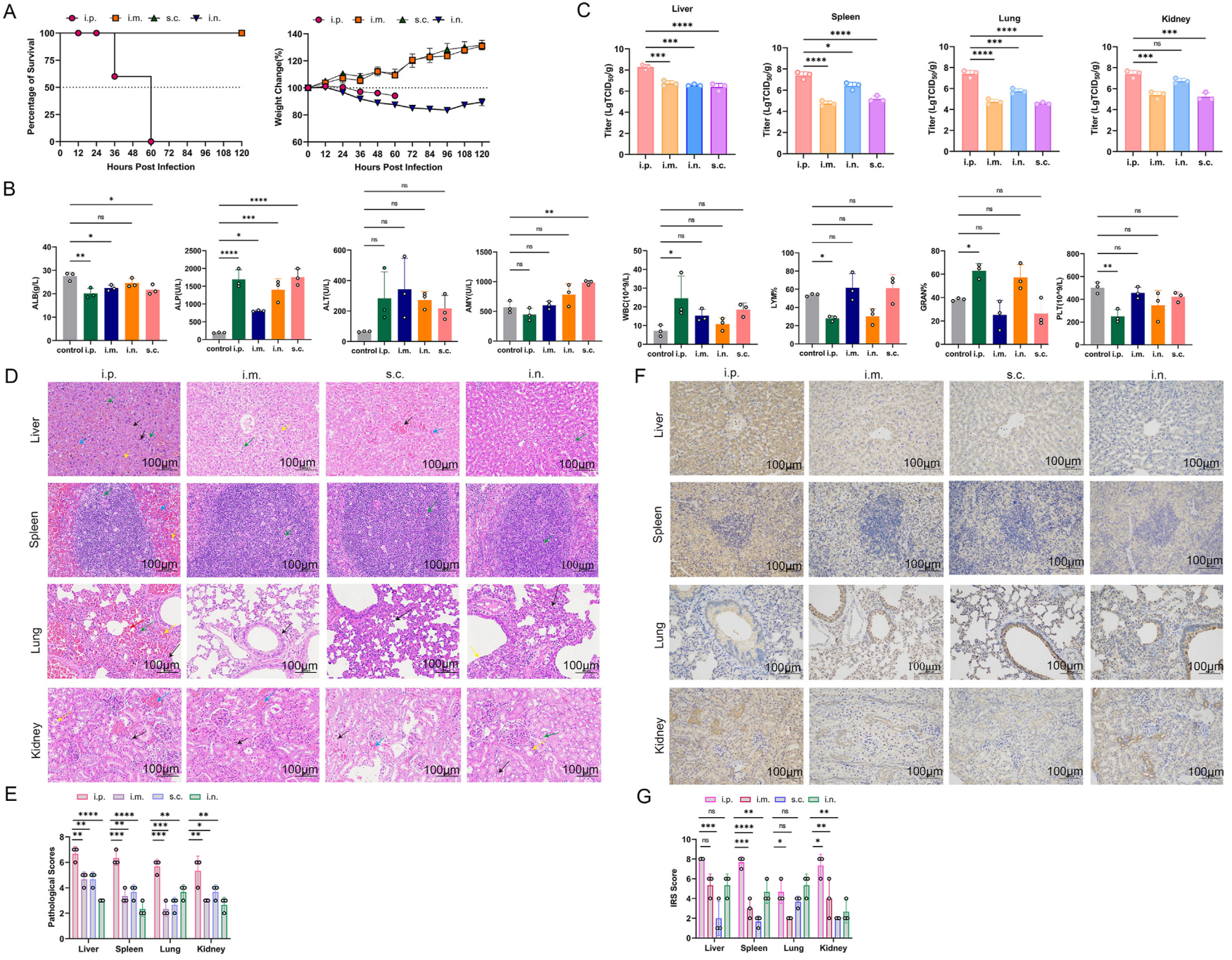

Fig. 5. Comparison of challenge route-dependent of Syrian hamster infected with VSV-EBOV/GP (10^7 $TCID_{50}$) via intraperitoneal (i.p.), subcutaneous (s.c.), intramuscular (i.m.), and intranasal (i.n.) route. Animals were monitored for weight changes and survival (**A**). **B** Blood biochemistry and blood cell count were analyzed at 1.5 days post-infection. **C** Viral loads including liver, spleen, lung, and kidney were determined at 1.5 days post-infection. **D, E** Histopathological changes of the liver, spleen, lung and kidney, and pathological scores at 1.5 days post-infection. Scale bar = 100 μm. Hepatic lesions including hepatocellular necrosis, nuclear fragmentation (black arrows), lymphocytic infiltration (blue arrows), granulocytic infiltration (green arrows), and hepatocellular steatosis (yellow arrows) were observed. Splenic lesions including cellular necrosis with nuclear fragmentation (blue arrows), neutrophilic infiltrate (green arrows), and bruising (yellow arrows) were observed. Lung lesions including alveolar hemorrhage (red arrows), granulocytic infiltration (green arrows), vascular stasis (yellow arrows) and moderate thickening of the alveolar wall (black arrows) were observed. Kidney lesions including necrosis of tubular epithelial cells (black arrows), eosinophilic material in the lumen of the tubules (yellow arrows), glomerular capillary stasis (red arrows), and interstitial capillary stasis (blue arrows) were observed. **F, G** Immunohistochemistry assays of the liver, spleen, lungs and kidneys, and histochemistry scores. Data presented as mean ± SEM. Statistical analyses were performed using One-way ANOVA. *, $P < 0.05$; **, $P < 0.01$; ***, $P < 0.001$; ****, $P < 0.0001$.

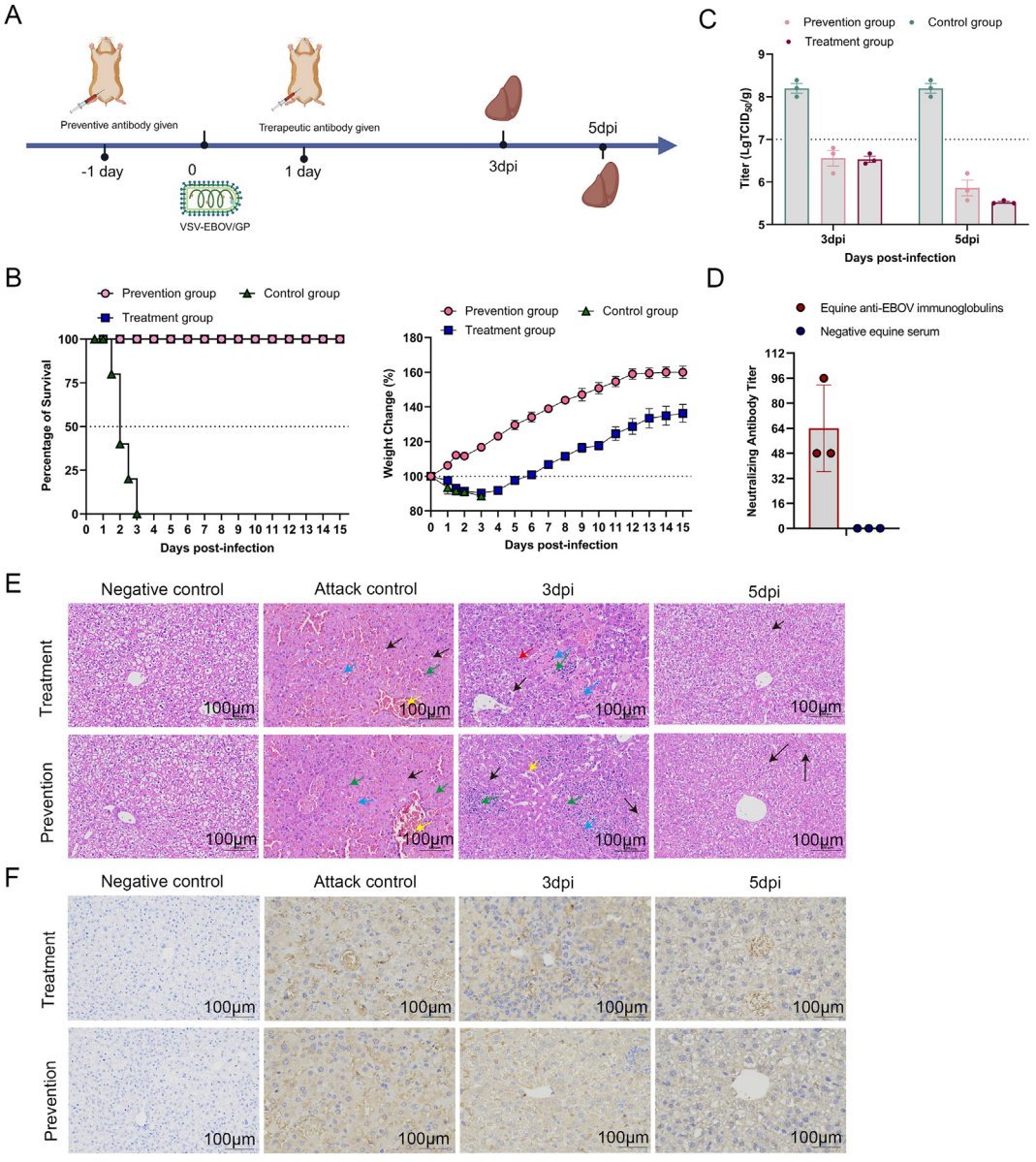

Fig. 6. Equine anti-EBOV immunoglobulins protect Syrian hamsters from lethal challenge of VSV-EBOV/GP. **A** Schematic representation of the preventive and therapeutic effects of antibodies evaluated in the Syrian hamster model. **B** Weight changes and percent of survival in treatment and prevention groups. **C** Viral loads were evaluated by $TCID_{50}$ in the liver at 3 days post-infection (dpi) and 5 dpi in treatment group, prevention group, and attack/control group. **D** The neutralizing antibody titer of Equine anti-EBOV immunoglobulins (starting concentration of 50 μg/mL, serially diluted two-fold from 1:3). **E** Pathology was examined, and representative hematoxylin and eosin staining images of liver are showed. Scale bar = 100 μm. Hepatic lesions including hepatocellular necrosis, nuclear fragmentation (black arrows), lymphocytic infiltration (blue arrows), granulocytic infiltration (green arrows), hepatocyte hydropic degeneration (red arrows), and a small amount of hepatocellular steatosis (yellow arrows) were observed. **F** Viral antigen in the liver of VSV-EBOV/GP-infected Syrian hamster in treatment group, prevention group, and attack group at 3 dpi and 5 dpi.

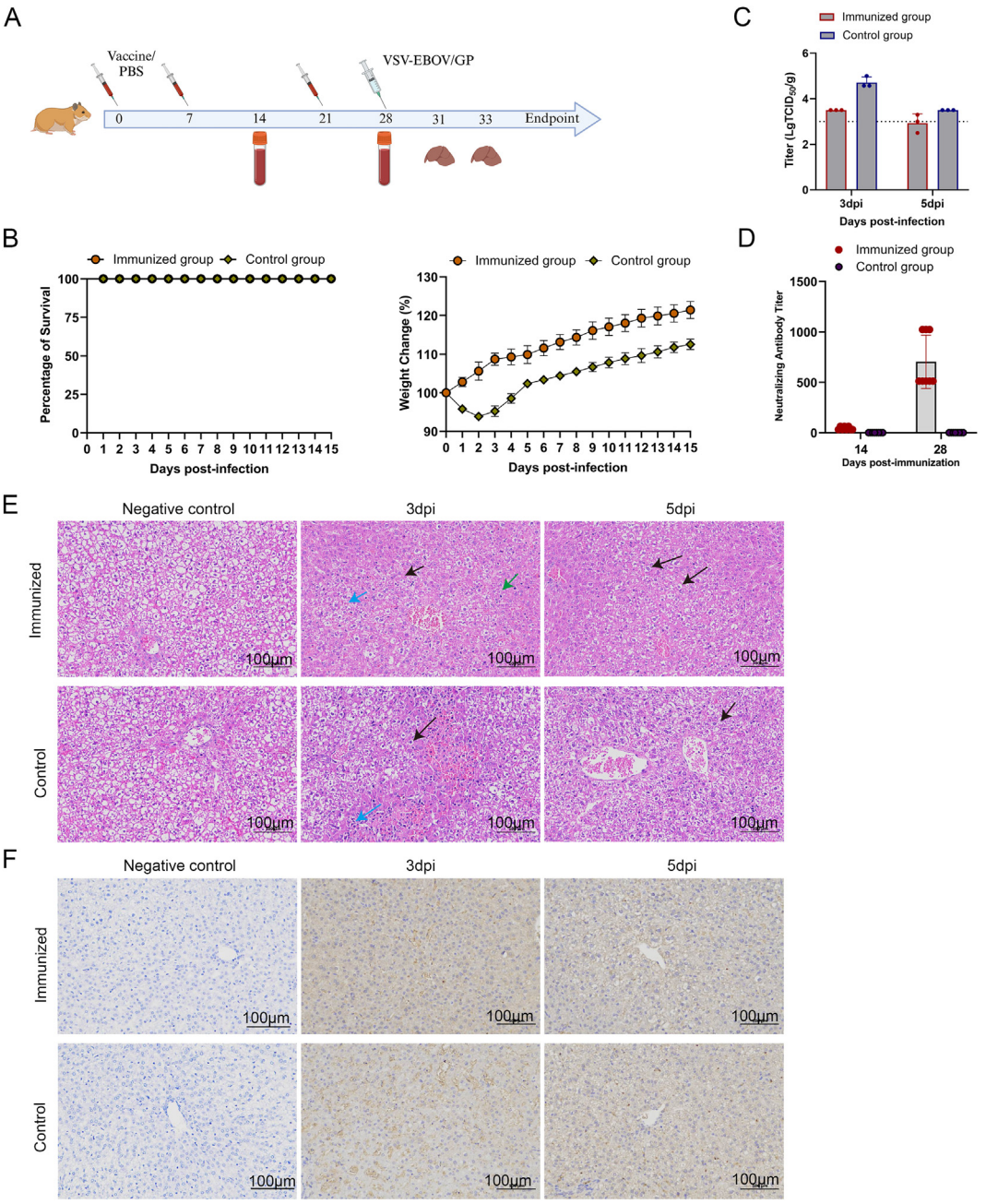

Fig. 7. Evaluation of the protective efficacy of EBOV GP Δmuc in lethal Syrian hamster model. **A** Schematic representation of the preventive effects of vaccination evaluated in the Syrian hamster model. **B** Weight change and percent of survival after VSV-EBOV/GP infection. **C** Viral loads were evaluated by $TCID_{50}$ in the liver at 3 days post-infection (dpi) and 5 dpi. **D** Serum neutralizing antibody following second and third immunization. **E** Representative hematoxylin and eosin stains of liver at 3 dpi and 5 dpi. Scale bar = 100 μm. Hepatic lesions including hepatocellular necrosis, nuclear fragmentation (black arrows), lymphocytic infiltration (blue arrows), and granulocytic infiltration (green arrows) were observed. **F** Viral antigen in the liver of VSV-EBOV/GP-infected Syrian hamster at 3 dpi and 5 dpi.

(Fig. 7A). All animals survived; the control group showed weight loss at 8% within 2 dpi and gradually regained in the following 12 days and the immunized group also conducted a sustainable weight increase at 20% (Fig. 7B). Furthermore, liver viral burden levels in the immunized group significantly decreased from 3 dpi to 5 dpi, and lower than in the control group (Fig. 7C). Additionally, there were significant increases in the serum-neutralizing antibody after the third immunization compared to the second (Fig. 7D). Overall, the livers exhibited hepatocellular necrosis and inflammatory cell infiltration at 3 dpi but showed alleviated symptoms at 5 dpi, and the control group was more severe than the immunized group (Fig. 7E). The positive antigens detected by immunohistochemistry also proved the above results (Fig. 7F). No deaths were observed in any of the groups of hamsters since these animals were 7–8 weeks old at the time of the challenge. The above results confirm that the hamster model also plays a role in assessing the preventive effect of vaccines.

4. Discussion

The clinical symptoms and progression of EVD are well-documented. However, the sporadic nature of its outbreaks, combined with its highly contagiousness and lethality, has led to limited clinical data for a thorough understanding of the immune response to EVD or establishing surrogates for protection. The lack of suitable animal models and the requirement for high containment labs also have impeded studies on

EBOV's pathogenesis and treatment. Therefore, constructing surrogate BSL-2 compliant EBOV and establishing models to replicate EVD disease will accelerate technological advances and breakthroughs confronting EVD.

VSV is a well-characterized model virus that has been extensively applied in viral vector vaccines, oncolytic viruses, and pseudo-virus packaging systems (Wang et al., 2023). It has a non-segmented negative-strand RNA genome that can be manipulated by reverse genetic approaches (Lawson et al., 1995). The most noteworthy design strategy, VSVΔG, involves replacing VSV G with foreign glycoprotein, resulting in a recombinant virus with altered cell and tissue tropism, depending on the foreign glycoproteins involved (Bukreyev et al., 2009; Geisbert and Feldmann, 2011). The above intrinsic properties provide the theoretical basis for the rational application of recombinant VSV-based surrogate virus for EBOV. Therefore, a series of recombinant VSV-based filoviruses were rescued and investigated in rodents in this study. Our results indicate that VSV-based recombinant virus shows potential as a surrogate viral platform, which may be applicable to other pathogens.

Previously, ferrets and non-human primates have been identified as naturally susceptible models of EBOV, which replicate certain aspects of human EVD (Bowen et al., 1978; Brasel et al., 2021; Cross et al., 2016; Ebihara et al., 2011; Geisbert et al., 2002; Kozak et al., 2016; Liu et al., 2023; Warren et al., 2020; Wong et al., 2018; Woolsey et al., 2022; Zumbrun et al., 2012). However, these models must be handled in BSL-4 containments. For convenience, accessibility and economy, surrogate models in small animal models under lower biosafety conditions are preferred. Unfortunately, conventional small animal models, such as mice, hamsters, and guinea pigs, were either insusceptible or less well susceptible to EBOV (Bowen et al., 1977; Bray, 2001; Bray et al., 1999; Simpson et al., 1968; Warfield et al., 2009). To address this obstacle, virus adaptation or immune-deficient animals were utilized, enabling EBOV's lethal infection. The virus adaptation approaches introduced additional mutants, which may distinguish it from the original virus. Immune-deficient animals compromise the host immune response, limiting their application for live vaccine evaluation (Banadyga et al., 2016; Bente et al., 2009; Bray et al., 1999; Connolly et al., 1999; Ebihara et al., 2006, 2013; Ryabchikova et al., 1996; Subbotina et al., 2010). Similarly, the insusceptibility of EBOV in rodents poses a challenge to applying the surrogate virus, as rodents may also resist the surrogate virus. In response, this study investigated the surrogate virus in terms of species-specific, age/gender-related, and challenge route-dependent manners. Among SD rats, BALB/c mice, guinea pigs, and Syrian hamsters, only 3-week-old female hamsters were uniformly lethal to VSV-EBOV/GP by i.p. injection. Specifically, this model replicated several aspects of human EVD, including weight loss, diarrhea, arched backs, depression, coarse coats, respiratory distress, loss of exploratory behavior, uniform lethality, multi-organ failure, along with abnormal blood parameters such as low WBC and PLT, elevated ALP and ALT, and viral load, suggesting systemic replication and hepatophilic of the virus, all of which have been observed in EVD patients and NHPs (Glaze et al., 2015; Jacob et al., 2020). Of particular note, infected hamsters experienced eye exudates, highly comparable to the optic nerve problems in infected humans (McWilliams et al., 2019). Previous studies have shown that Syrian hamsters infected with mouse-adapted EBOV (MA-EBOV) developed clinical signs of EVD, such as ruffled fur and reduced activity at 3 dpi and succumbed to the disease at 4–5 dpi (Ebihara et al., 2013). Severe coagulation disorders, thrombocytopenia, and high viral loads in the body were also observed as histopathological changes, including inflammatory cell infiltration, cell necrosis, apoptosis, and severe liver damage. Instead of MA-EBOV, we used VSV-EBOV/GP to infect the Syrian hamster, which completely replicated the above symptoms and operated under BSL-2 conditions for preclinical evaluation of EBOV antibodies and vaccines.

In addition, two previously established medical countermeasures for EVD, including therapeutic equine-origin immunoglobulin antibodies and preventive subunit vaccines, were validated in this model (Wang et al., 2019). The results of the neutralization assay showed that the equine anti-EBOV immunoglobulin exhibited complete neutralizing activity against VSV-EBOV/GP at a concentration of 0.15 (μg/mL). Equine anti-EBOV immunoglobulins protected Syrian hamsters from the lethal challenge of the surrogate virus, with a protective efficacy of 100%. Regarding the subunit vaccine, EBOV GP Δmuc provided protective efficacy in hamsters, presented as reduced viral loads and alleviated pathological damage. The above results suggest that the surrogate model would be an economical and efficient choice for the preliminary and rapid screening of medical countermeasures against EBOV.

Generally, we established a surrogate model with precise prerequisites and validated medical countermeasures, but the underlying mechanisms contributing to pathogenesis remain unknown. For instance, in line with previous studies, we confirmed that i.p. injection is the most effective infection route in rodents, but further clarification on potential mechanisms is needed (Banadyga et al., 2016; Siragam et al., 2018; St Claire et al., 2017). This delivery route-dependent phenomenon may be attributed to the rapid uptake of the virus by phagocytic cells in the peritoneal cavity, lack of recruited innate immunity, and systemic distribution of the surrogate virus. Moreover, due to the hepatophilic nature of EBOV, the i.p. injection route allows rapid and timely exposure of hepatocytes compared to other delivery routes, together with the rapid replication capability of VSV, leading to multiorgan failure and fatal outcome (Bradfute et al., 2010; Ebihara et al., 2013). We also observed that the lethality of VSV-EBOV/GP in Syrian hamsters is age-related; 3-week-old female Syrian hamsters were the most uniformly lethal following infection with VSV-EBOV/GP. Lethal meningoencephalitis in neonatal C57BL/6 mice challenged with VSV-EBOV pseudo-virus has been reported (Lee et al., 2021), suggesting that 3-week-old Syrian hamsters, being in the weaning stage and having incomplete immunity, are probably less able to fight the virus than the adult Syrian hamster, thus resulting in more uniformly lethal. Previous studies have shown that WT VSV replicated efficiently in multiple organs and led to fatal infection in hamsters (Fultz and Holland, 1985; Fultz et al., 1981). Moreover, the virus entry and pathogenicity were proved to be glycoprotein-associated(Beier et al., 2011, 2013; Garbutt et al., 2004; Muik et al., 2014; Wollmann et al., 2015). Our study further confirmed this phenomenon. As VSV-EBOV/GP, but not VSV-SUDV/GP and VSV-LASV/GP, could cause lethal infection in Syrian hamsters. Compared with WT VSV, VSV-EBOV/GP showed marked hepatophilic behavior in hamsters. Taken together, the pathogenicity of VSV-EBOV/GP was glycoprotein-associated. The interaction between foreign glycoprotein and the VSV backbone and its corresponding impact on pathogenicity should be further investigated in further studies.

5. Conclusions

Overall, this study provides a surrogate model of EVD with high cost-effectiveness, which were uniformly lethal and replicated several critical aspects of human EVD. This model enabled rapid preclinical evaluation of medical countermeasures against EBOV under BLS-2 conditions. The surrogate virus and matched hamster EVD model will improve the security and economy of the research in the EBOV field. Reasonable application of the surrogate model would accelerate technological advances and breakthroughs against EVD.

Data availability

All data generated or analyzed during this study are included in this published article.

Ethics statement

Animal experiments were performed at the BSL-2 facility and approved by the animal experimental committee of the Laboratory

Animal Center, Changchun Veterinary Research Institute, Chinese Academy of Agricultural Science (approval number: IACUC of AMMS-11-2020 -020).

Author contributions

Wanying Yang: data curation, investigation, writing-original draft. Wujian Li: investigation, software. Wujie Zhou: conceptualization, methodology. Shen Wang: writing-review & editing. Weiqi Wang: software, methodology. Zhenshan Wang: Validation. Na Feng: supervision, Tiecheng Wang: project administration. Ying Xie: supervision, writing-review & editing. Yongkun Zhao: funding acquisition. Feihu Yan: funding acquisition, writing-review & editing. Xianzhu Xia: conceptualization, supervision.

Conflict of interest

The authors declare that they have no conflict of interest.

Acknowledgements

This work was supported by National Key R&D Program of China (grant number 2023YFC2605500); Jilin Province Youth Talent Support Project (grant number QT202208); and the Ministry of Science and Technology of the People's Republic of China (grant number 2022YFC0867900); and Nation Key Research and Development Program of China, New technology of rapid of pathogens in laboratory animals (grant number 2021YFF07033600).

References

Banadyga, L., Dolan, M.A., Ebihara, H., 2016. Rodent-adapted filoviruses and the Molecular basis of pathogenesis. J. Mol. Biol. 428, 3449–3466.
Baseler, L., Chertow, D.S., Johnson, K.M., Feldmann, H., Morens, D.M., 2017. The pathogenesis of ebola virus disease. Annu. Rev. Pathol. 12, 387–418.
Beier, K.T., Saunders, A., Oldenburg, I.A., Miyamichi, K., Akhtar, N., Luo, L., Whelan, S.P., Sabatini, B., Cepko, C.L., 2011. Anterograde or retrograde transsynaptic labeling of CNS neurons with vesicular stomatitis virus vectors. Proc. Natl. Acad. Sci. U.S.A. 108, 15414–15419.
Beier, K.T., Saunders, A.B., Oldenburg, I.A., Sabatini, B.L., Cepko, C.L., 2013. Vesicular stomatitis virus with the rabies virus glycoprotein directs retrograde transsynaptic transport among neurons in vivo. Front. Neural Circ. 7, 11.
Benonisson, H., Altıntaş, I., Sluijter, M., Verploegen, S., Labrijn, A.F., Schuurhuis, D.H., Houtkamp, M.A., Verbeek, J.S., Schuurman, J., van Hall, T., 2019. CD3-Bispecific antibody therapy Turns Solid tumors into inflammatory Sites but Does not Install protective memory. Mol. Cancer Therapeut. 18, 312–322.
Bente, D., Gren, J., Strong, J.E., Feldmann, H., 2009. Disease modeling for ebola and marburg viruses. Dis. Model. Mech. 2, 12–17.
Bowen, E.T., Lloyd, G., Harris, W.J., Platt, G.S., Baskerville, A., Vella, E.E., 1977. Viral haemorrhagic fever in southern Sudan and northern Zaire. Preliminary studies on the aetiological agent. Lancet 1, 571–573.
Bowen, E.T., Platt, G.S., Simpson, D.I., McArdell, L.B., Raymond, R.T., 1978. Ebola haemorrhagic fever: experimental infection of monkeys. Trans. R. Soc. Trop. Med. Hyg. 72, 188–191.
Bradfute, S.B., Swanson, P.E., Smith, M.A., Watanabe, E., McDunn, J.E., Hotchkiss, R.S., Bavari, S., 2010. Mechanisms and consequences of ebolavirus-induced lymphocyte apoptosis. J. Immunol. 184, 327–335.
Bradfute, S.B., Warfield, K.L., Bray, M., 2012. Mouse models for filovirus infections. Viruses 4, 1477–1508.
Brasel, T., Comer, J.E., Massey, S., Smith, J., Smith, J., Hyde, M., Kocsis, A., Gainey, M., Niemuth, N., Triplett, C., Rudge Jr., T., 2021. Mucosal challenge ferret models of ebola virus disease. Pathogens 10, 292.
Bray, M., 2001. The role of the Type I interferon response in the resistance of mice to filovirus infection. J. Gen. Virol. 82, 1365–1373.
Bray, M., Davis, K., Geisbert, T., Schmaljohn, C., Huggins, J., 1999. A mouse model for evaluation of prophylaxis and therapy of Ebola hemorrhagic fever. J. Infect. Dis. 179 (Suppl. 1), S248–S258.
Bukreyev, A., Marzi, A., Feldmann, F., Zhang, L., Yang, L., Ward, J.M., Dorward, D.W., Pickles, R.J., Murphy, B.R., Feldmann, H., Collins, P.L., 2009. Chimeric human parainfluenza virus bearing the Ebola virus glycoprotein as the sole surface protein is immunogenic and highly protective against Ebola virus challenge. Virology 383, 348–361.
Coltart, C.E., Lindsey, B., Ghinai, I., Johnson, A.M., Heymann, D.L., 2017. The Ebola outbreak, 2013-2016: old lessons for new epidemics. Phil. Trans. Roy. Soc. Lond. B Biol. Sci. 372, 20160297.
Connolly, B.M., Steele, K.E., Davis, K.J., Geisbert, T.W., Kell, W.M., Jaax, N.K., Jahrling, P.B., 1999. Pathogenesis of experimental Ebola virus infection in Guinea pigs. J. Infect. Dis. 179 (Suppl. 1), S203–S217.
Cooper, T.K., Huzella, L., Johnson, J.C., Rojas, O., Yellayi, S., Sun, M.G., Bavari, S., Bonilla, A., Hart, R., Jahrling, P.B., Kuhn, J.H., Zeng, X., 2018. Histology, immunohistochemistry, and in situ hybridization reveal overlooked Ebola virus target tissues in the Ebola virus disease Guinea pig model. Sci. Rep. 8, 1250.
Cross, R.W., Mire, C.E., Borisevich, V., Geisbert, J.B., Fenton, K.A., Geisbert, T.W., 2016. The domestic ferret (Mustela putorius furo) as a lethal infection model for 3 species of ebolavirus. J. Infect. Dis. 214, 565–569.
Ebihara, H., Rockx, B., Marzi, A., Feldmann, F., Haddock, E., Brining, D., LaCasse, R.A., Gardner, D., Feldmann, H., 2011. Host response dynamics following lethal infection of rhesus macaques with Zaire ebolavirus. J. Infect. Dis. 204 (Suppl. 3), S991–S999.
Ebihara, H., Takada, A., Kobasa, D., Jones, S., Neumann, G., Theriault, S., Bray, M., Feldmann, H., Kawaoka, Y., 2006. Molecular determinants of Ebola virus virulence in mice. PLoS Pathog. 2, e73.
Ebihara, H., Zivcec, M., Gardner, D., Falzarano, D., LaCasse, R., Rosenke, R., Long, D., Haddock, E., Fischer, E., Kawaoka, Y., Feldmann, H., 2013. A Syrian golden hamster model recapitulating ebola hemorrhagic fever. J. Infect. Dis. 207, 306–318.
Feldmann, H., Sprecher, A., Geisbert, T.W., 2020. Ebola. N. Engl. J. Med. 382, 1832–1842.
Fultz, P.N., Holland, J.J., 1985. Differing responses of hamsters to infection by vesicular stomatitis virus Indiana and New Jersey serotypes. Virus Res. 3, 129–140.
Fultz, P.N., Shadduck, J.A., Kang, C.Y., Streilein, J.W., 1981. Genetic analysis of resistance to lethal infections of vesicular stomatitis virus in Syrian hamsters. Infect. Immun. 32, 1007–1013.
Garbutt, M., Liebscher, R., Wahl-Jensen, V., Jones, S., Möller, P., Wagner, R., Volchkov, V., Klenk, H.D., Feldmann, H., Ströher, U., 2004. Properties of replication-competent vesicular stomatitis virus vectors expressing glycoproteins of filoviruses and arenaviruses. J. Virol. 78, 5458–5465.
Geisbert, T.W., Feldmann, H., 2011. Recombinant vesicular stomatitis virus-based vaccines against Ebola and Marburg virus infections. J. Infect. Dis. 204 (Suppl. 3), S1075–S1081.
Geisbert, T.W., Pushko, P., Anderson, K., Smith, J., Davis, K.J., Jahrling, P.B., 2002. Evaluation in nonhuman primates of vaccines against Ebola virus. Emerg. Infect. Dis. 8, 503–507.
Glaze, E.R., Roy, M.J., Dalrymple, L.W., Lanning, L.L., 2015. A comparison of the pathogenesis of marburg virus disease in humans and nonhuman primates and evaluation of the suitability of these animal models for predicting clinical efficacy under the 'animal rule'. Comp. Med. 65, 241–259.
Jacob, S.T., Crozier, I., Fischer, W.A., Hewlett, A., Kraft, C.S., Vega, M.A., Soka, M.J., Wahl, V., Griffiths, A., Bollinger, L., Kuhn, J.H., 2020. Ebola virus disease. Nat. Rev. Dis. Prim. 6, 13.
Johnson, D.M., Brasel, T., Massey, S., Smith, J., Garron, T., Wallace, S., Yu, X., Beasley, D.W., Comer, J.E., 2023. Characterization of ebola virus mucosal challenge routes in cynomolgus macaques. J. Virol. 97, e0188822.
Keck, Z.Y., Enterlein, S.G., Howell, K.A., Vu, H., Shulenin, S., Warfield, K.L., Froude, J.W., Araghi, N., Douglas, R., Biggins, J., Lear-Rooney, C.M., Wirchnianski, A.S., Lau, P., Wang, Y., Herbert, A.S., Dye, J.M., Glass, P.J., Holtsberg, F.W., Foung, S.K., Aman, M.J., 2016. Macaque monoclonal antibodies targeting novel conserved epitopes within filovirus glycoprotein. J. Virol. 90, 279–291.
Kozak, R., He, S., Kroeker, A., de La Vega, M.A., Audet, J., Wong, G., Urfano, C., Antonation, K., Embury-Hyatt, C., Kobinger, G.P., Qiu, X., 2016. Ferrets infected with bundibugyo virus or ebola virus recapitulate important aspects of human filovirus disease. J. Virol. 90, 9209–9223.
Lawson, N.D., Stillman, E.A., Whitt, M.A., Rose, J.K., 1995. Recombinant vesicular stomatitis viruses from DNA. Proc. Natl. Acad. Sci. U.S.A. 92, 4477–4481.
Lee, H.N., McWilliams, I.L., Lewkowicz, A.P., Engel, K., Ireland, D.D.C., Kelley-Baker, L., Thacker, S., Piccardo, P., Manangeeswaran, M., Verthelyi, D., 2021. Characterization of the therapeutic effect of antibodies targeting the Ebola glycoprotein using a novel BSL2-compliant rVSVΔG-EBOV-GP infection model. Emerg. Microb. Infect. 10, 2076–2089.
Leligdowicz, A., Fischer, W.A., Uyeki, T.M., Fletcher, T.E., Adhikari, N.K., Portella, G., Lamontagne, F., Clement, C., Jacob, S.T., Rubinson, L., Vanderschuren, A., Hajek, J., Murthy, S., Ferri, M., Crozier, I., Ibrahima, E., Lamah, M.C., Schieffelin, J.S., Brett-Major, D., Bausch, D.G., Shindo, N., Chan, A.K., O'Dempsey, T., Mishra, S., Jacobs, M., Dickson, S., Lyon, G.M., Fowler, R.A., 2016. Ebola virus disease and critical illness. Crit. Care 20, 217.
Liu, D.X., Pahar, B., Cooper, T.K., Perry, D.L., Xu, H., Huzella, L.M., Adams, R.D., Hischak, A.M.W., Hart, R.J., Bernbaum, R., Rivera, D., Anthony, S., Claire, M.S., Byrum, R., Cooper, K., Reeder, R., Kurtz, J., Hadley, K., Wada, J., Crozier, I., Worwa, G., Bennett, R.S., Warren, T., Holbrook, M.R., Schmaljohn, C.S., Hensley, L.E., 2023. Ebola virus disease features hemophagocytic lymphohistiocytosis/macrophage activation syndrome in the rhesus macaque model. J. Infect. Dis. 228, 371–382.
Manangeeswaran, M., Ireland, D.D., Verthelyi, D., 2016. Zika (PRVABC59) infection is associated with T cell infiltration and neurodegeneration in CNS of immunocompetent neonatal C57Bl/6 mice. PLoS Pathog. 12, e1006004.
Martin, B., Canard, B., Decroly, E., 2017. Filovirus proteins for antiviral drug discovery: structure/function bases of the replication cycle. Antivir. Res. 141, 48–61.
Martin, B., Hoenen, T., Canard, B., Decroly, E., 2016. Filovirus proteins for antiviral drug discovery: a structure/function analysis of surface glycoproteins and virus entry. Antivir. Res. 135, 1–14.
McWilliams, I.L., Kielczewski, J.L., Ireland, D.D.C., Sykes, J.S., Lewkowicz, A.P., Konduru, K., Xu, B.C., Chan, C.C., Caspi, R.R., Manangeeswaran, M., Verthelyi, D., 2019. Pseudovirus rVSVΔG-ZEBOV-GP infects neurons in retina and CNS, causing apoptosis and neurodegeneration in neonatal mice. Cell Rep. 26, 1718–1726.e1714.

Muik, A., Stubbert, L.J., Jahedi, R.Z., Geiβ, Y., Kimpel, J., Dold, C., Tober, R., Volk, A., Klein, S., Dietrich, U., Yadollahi, B., Falls, T., Miletic, H., Stojdl, D., Bell, J.C., von Laer, D., 2014. Re-engineering vesicular stomatitis virus to abrogate neurotoxicity, circumvent humoral immunity, and enhance oncolytic potency. Cancer Res. 74, 3567–3578.

Nakayama, E., Saijo, M., 2013. Animal models for Ebola and Marburg virus infections. Front. Microbiol. 4, 267.

Nicastri, E., Kobinger, G., Vairo, F., Montaldo, C., Mboera, L.E.G., Ansunama, R., Zumla, A., Ippolito, G., 2019. Ebola virus disease: epidemiology, clinical features, management, and prevention. Infect. Dis. Clin. 33, 953–976.

Ryabchikova, E., Kolesnikova, L., Smolina, M., Tkachev, V., Pereboeva, L., Baranova, S., Grazhdantseva, A., Rassadkin, Y., 1996. Ebola virus infection in Guinea pigs: presumable role of granulomatous inflammation in pathogenesis. Arch. Virol. 141, 909–921.

Shantha, J.G., Crozier, I., Hayek, B.R., Bruce, B.B., Gargu, C., Brown, J., Fankhauser, J., Yeh, S., 2017. Ophthalmic manifestations and causes of vision impairment in ebola virus disease survivors in monrovia, Liberia. Ophthalmology 124, 170–177.

Simpson, D.I., Zlotnik, I., Rutter, D.A., 1968. Vervet monkey disease. Experiment infection of Guinea pigs and monkeys with the causative agent. Br. J. Exp. Pathol. 49, 458–464.

Siragam, V., Wong, G., Qiu, X.G., 2018. Animal models for filovirus infections. Zool. Res. 39, 15–24.

St Claire, M.C., Ragland, D.R., Bollinger, L., Jahrling, P.B., 2017. Animal models of ebolavirus infection. Comp. Med. 67, 253–262.

Subbotina, E., Dadaeva, A., Kachko, A., Chepurnov, A., 2010. Genetic factors of Ebola virus virulence in Guinea pigs. Virus Res. 153, 121–133.

Wahl-Jensen, V., Bollinger, L., Safronetz, D., de Kok-Mercado, F., Scott, D.P., Ebihara, H., 2012. Use of the Syrian hamster as a new model of ebola virus disease and other viral hemorrhagic fevers. Viruses 4, 3754–3784.

Wang, H., Wong, G., Zhu, W., He, S., Zhao, Y., Yan, F., Rahim, M.N., Bi, Y., Zhang, Z., Cheng, K., Jin, H., Cao, Z., Zheng, X., Gai, W., Bai, J., Chen, W., Zou, Y., Gao, Y., Gao, G.F., Yang, S., Xia, X., Qiu, X., 2019. Equine-origin immunoglobulin fragments protect nonhuman primates from ebola virus disease. J. Virol. 93, e01548-18.

Wang, S., Liang, B., Wang, W., Li, L., Feng, N., Zhao, Y., Wang, T., Yan, F., Yang, S., Xia, X., 2023. Viral vectored vaccines: design, development, preventive and therapeutic applications in human diseases. Signal Transduct. Targeted Ther. 8, 149.

Wang, S., Zhang, C., Liang, B., Wang, W., Feng, N., Zhao, Y., Wang, T., Guo, Z., Yan, F., Yang, S., Xia, X., 2022. Characterization of immune response diversity in rodents vaccinated with a vesicular stomatitis virus vectored COVID-19 vaccine. Viruses 14, 1127.

Warfield, K.L., Bradfute, S.B., Wells, J., Lofts, L., Cooper, M.T., Alves, D.A., Reed, D.K., VanTongeren, S.A., Mech, C.A., Bavari, S., 2009. Development and characterization of a mouse model for Marburg hemorrhagic fever. J. Virol. 83, 6404–6415.

Warren, T., Zumbrun, E., Weidner, J.M., Gomba, L., Rossi, F., Bannister, R., Tarrant, J., Reed, M., Lee, E., Raymond, J.L., Wells, J., Shamblin, J., Wetzel, K., Donnelly, G., Van Tongeren, S., Lackemeyer, N., Steffens, J., Kimmel, A., Garvey, C., Bloomfield, H., Blair, C., Singh, B., Bavari, S., Cihlar, T., Porter, D., 2020. Characterization of ebola virus disease (EVD) in rhesus monkeys for development of EVD therapeutics. Viruses 12, 92.

Wollmann, G., Drokhlyansky, E., Davis, J.N., Cepko, C., van den Pol, A.N., 2015. Lassa-vesicular stomatitis chimeric virus safely destroys brain tumors. J. Virol. 89, 6711–6724.

Wong, G., Leung, A., He, S., Cao, W., De La Vega, M.A., Griffin, B.D., Soule, G., Kobinger, G.P., Kobasa, D., Qiu, X., 2018. The makona variant of ebola virus is highly lethal to immunocompromised mice and immunocompetent ferrets. J. Infect. Dis. 218, S466–s470.

Woolsey, C., Fears, A.C., Borisevich, V., Agans, K.N., Dobias, N.S., Prasad, A.N., Deer, D.J., Geisbert, J.B., Fenton, K.A., Geisbert, T.W., Cross, R.W., 2022. Natural history of Sudan ebolavirus infection in rhesus and cynomolgus macaques. Emerg. Microb. Infect. 11, 1635–1646.

Xie, P., Zhang, M., He, S., Lu, K., Chen, Y., Xing, G., Lu, Y., Liu, P., Li, Y., Wang, S., Chai, N., Wu, J., Deng, H., Wang, H.R., Cao, Y., Zhao, F., Cui, Y., Wang, J., He, F., Zhang, L., 2014. The covalent modifier Nedd8 is critical for the activation of Smurf1 ubiquitin ligase in tumorigenesis. Nat. Commun. 5, 3733.

Yan, F., He, S., Banadyga, L., Zhu, W., Zhang, H., Rahim, M.N., Collignon, B., Senthilkumaran, C., Embury-Hyatt, C., Qiu, X., 2019. Characterization of Reston virus infection in ferrets. Antivir. Res. 165, 1–10.

Zumbrun, E.E., Bloomfield, H.A., Dye, J.M., Hunter, T.C., Dabisch, P.A., Garza, N.L., Bramel, N.R., Baker, R.J., Williams, R.D., Nichols, D.K., Nalca, A., 2012. A characterization of aerosolized Sudan virus infection in African green monkeys, cynomolgus macaques, and rhesus macaques. Viruses 4, 2115–2136.